scientific reports

Check for updates

OPEN

Investigating the effects of stereotactic body radiation therapy on pancreatic tumor hypoxia and microvasculature in an orthotopic mouse model using intravital fluorescence microscopy

Timothy Samuel[1,2], Sara Rapic[1], Patricia E. Lindsay[1,3] & Ralph S. DaCosta[1,2]✉

Despite decades of improvements in cytotoxic therapy, the current standard of care for locally advanced pancreatic cancer (LAPC) provides, on average, only a few months of survival benefit. Stereotactic Body Radiation Therapy (SBRT), a technique that accurately delivers high doses of radiation to tumors in fewer fractions, has emerged as a promising therapy to improve local control of LAPC; however, its effects on the tumor microenvironment and hypoxia remain poorly understood. To explore how SBRT affects pancreatic tumors, we combined an orthotopic mouse model of pancreatic cancer with an intravital microscopy platform to visualize changes to the in vivo tumor microenvironment in real-time. Mice received SBRT (5 × 8 Gy) or were left untreated, and were imaged before and 1, 4, 7, and 14 days after treatment (n = 7/group). A fluorescent human pancreatic cancer cell line (BxPC3-DsRed) engineered to express GFP under hypoxic conditions (driven by hypoxia-inducible factor, HIF) was used to monitor tumor hypoxia. Immunohistochemical staining was also performed on tissues to validate in vivo data. Our findings demonstrate a persistent decrease in pancreatic tumor hypoxia as early as one day after SBRT. This coincided with a decrease in both tumor cell proliferation and cell density in the SBRT group. Reduced demand for oxygen after SBRT (due to cell death and growth arrest from treatment) significantly contributed to reoxygenation of the pancreatic TME. Understanding how this reoxygenation phenomenon occurs in a dose-dependent manner will help improve dosing and fractionation schemes for clinical SBRT.

Pancreatic cancer is a lethal malignancy with a median survival of less than 1 year[1]. While surgical resection remains the only curable treatment option, over 80% of cases are unresectable[2]. This leaves most patients with few effective treatment options and a 5-year survival rate of ~2%[3]. In addition to cytotoxic therapies, conventionally fractionated radiotherapy (CFRT) has been used to treat locally advanced pancreatic cancer (LAPC) but is associated with significant treatment burden (typically given over several weeks) and only provides a marginal improvement in overall survival[4–7]. Recent advances in image guidance have enabled techniques like stereotactic body radiation therapy (SBRT) to deliver higher doses of radiation in fewer treatment fractions while minimizing toxicity to surrounding organs[8,9]. Emerging data on SBRT for pancreatic tumors has shown promising local control rates ranging from 70 to 100%[8–16] as well as increased overall survival compared to CFRT or chemotherapy alone[4–6]. Nevertheless, treatment failure remains a significant issue[17]. With the advent of high-dose, hypo-fractionated radiotherapy (or SBRT), several questions remain about the optimal dose of ionizing radiation, treatment schedule, and radiobiological effects on the pancreatic tumor microenvironment (TME)[18,19].

Traditionally, our understanding of the radiobiological effects of radiotherapy on tumors has been focused on tumor cell death, typically mediated by radiation-induced DNA damage[20]. However, studies over the past decade have shown that the TME plays a significant role in treatment response following high-dose

[1]Princess Margaret Cancer Centre, University Health Network, Toronto, Canada. [2]Department of Medical Biophysics, University of Toronto, Toronto, Canada. [3]Department of Radiation Oncology, University of Toronto, Toronto, Canada. ✉email: ralph.dacosta@uhn.ca

radiotherapy, improving (or sometimes limiting) tumor control[20–25]. Doses of ionizing radiation greater than 10 Gy per fraction have been shown to impact not only tumor cells, but also many non-malignant cells that make up the TME. For example, radiation doses greater than 10 Gy are associated with severe vascular damage leading to indirect tumor cell death and increased tumor hypoxia[24,26–28]. This differs from the traditional concept of reoxygenation in CFRT, as successive treatment fractions reoxygenate hypoxic cells, improving treatment effect[29,30]. Moreover, many studies have demonstrated M2 polarization of tumor-associated macrophages after treatment with high-dose radiation regimens, potentially conferring a more aggressive tumor phenotype[31–33]. It is still unclear whether this phenomenon is a result of increased tumor hypoxia resulting from treatment[34] or occurs through an independent pathway. Improving our understanding of the effects of SBRT on pancreatic tumor hypoxia and the TME may help improve the design of such radiation treatments and determine optimal dosing schedules.

In this study, we aimed to develop and validate a dually fluorescent pancreatic tumor cell line to simultaneously monitor tumor response to SBRT in vivo and assess tumor cell hypoxia in an orthotopic mouse model of pancreatic cancer. To monitor the response of pancreatic tumors to SBRT, we designed and surgically implanted a transparent glass pancreatic imaging window into the abdomen of mice to permit longitudinal intravital fluorescence microscopy (IVFM) (Fig. 1, see Methods section for details). This technique enabled direct (optical) imaging of orthotopically implanted DsRed fluorescent human pancreatic cancer cells (BxPC3) at cellular resolution in situ, and within the same animal longitudinally for up to four weeks. This novel capability builds upon previous advancements in intravital imaging, which facilitate long-term visualization of dynamic processes at the cellular level in vivo[35–38], overcoming the limitations of static ex vivo tissue studies requiring animals to be euthanized at various time points.

We engineered BxPC3-DsRed cells to express a GFP fluorescent reporter activated under hypoxic conditions, enabling fluorescence-based visualization and quantification of tumor cell hypoxia in vivo[39]. In addition, Allophycocyanin (APC)-conjugated anti-CD31 fluorescent dye was intravenously injected into our mouse model before each imaging session to label vascular endothelial cells, allowing for simultaneous visualization of the tumor microvasculature in vivo in the same animal. Pancreatic tumors in mice were treated with SBRT (5 daily fractions of 8 Gy, or '5 × 8 Gy') using a small animal x-ray micro-irradiator to simulate a typical SBRT dose regimen for LAPC patients[40] (Fig. 2, see Methods section for details). Our results demonstrated a decrease in tumor cell hypoxia as early as 1 day after SBRT is delivered to the tumor. This coincided with a decrease in both

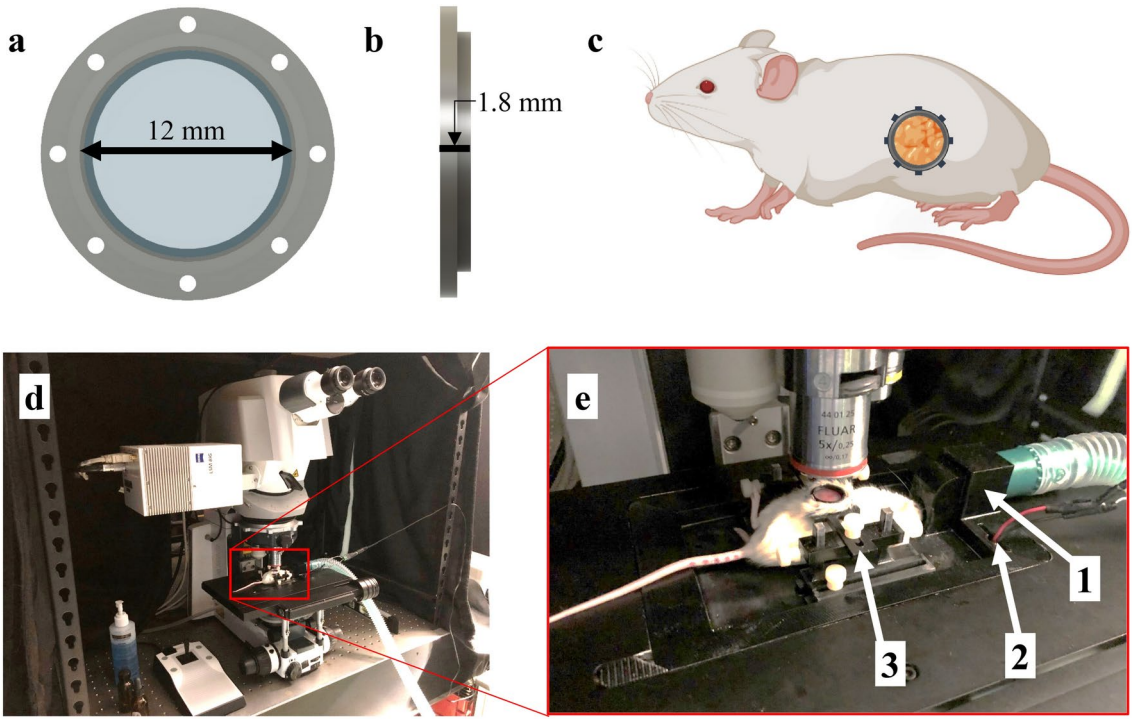

Fig. 1. Surgically implanted abdominal imaging window allows longitudinal intravital imaging of pancreatic tumors in vivo. (**a**,**b**) Computer-aided design (CAD) of an abdominal pancreatic imaging window (PIW) frame holding a circular glass coverslip (12 mm diameter). (**c**) Diagram of a mouse (using BioRender.com) indicating the anatomical location of the surgically implanted PIW. The PIW was 3D-printed with biocompatible, acrylonitrile butadiene styrene (ABS) plastic and surgically implanted over the tumor site, providing longitudinal imaging access to the pancreas in vivo. (**d**) Photo of laser-scanning confocal/multiphoton microscope with (**e**) a custom, 3D-printed stage insert to stabilize the animal for anesthesia and imaging. The stage is equipped with (1) a gas anesthesia port, (2) an electrical heating element and (3) a holder to minimize motion artifacts during imaging. This figure was originally published by Samuel et al.[39].

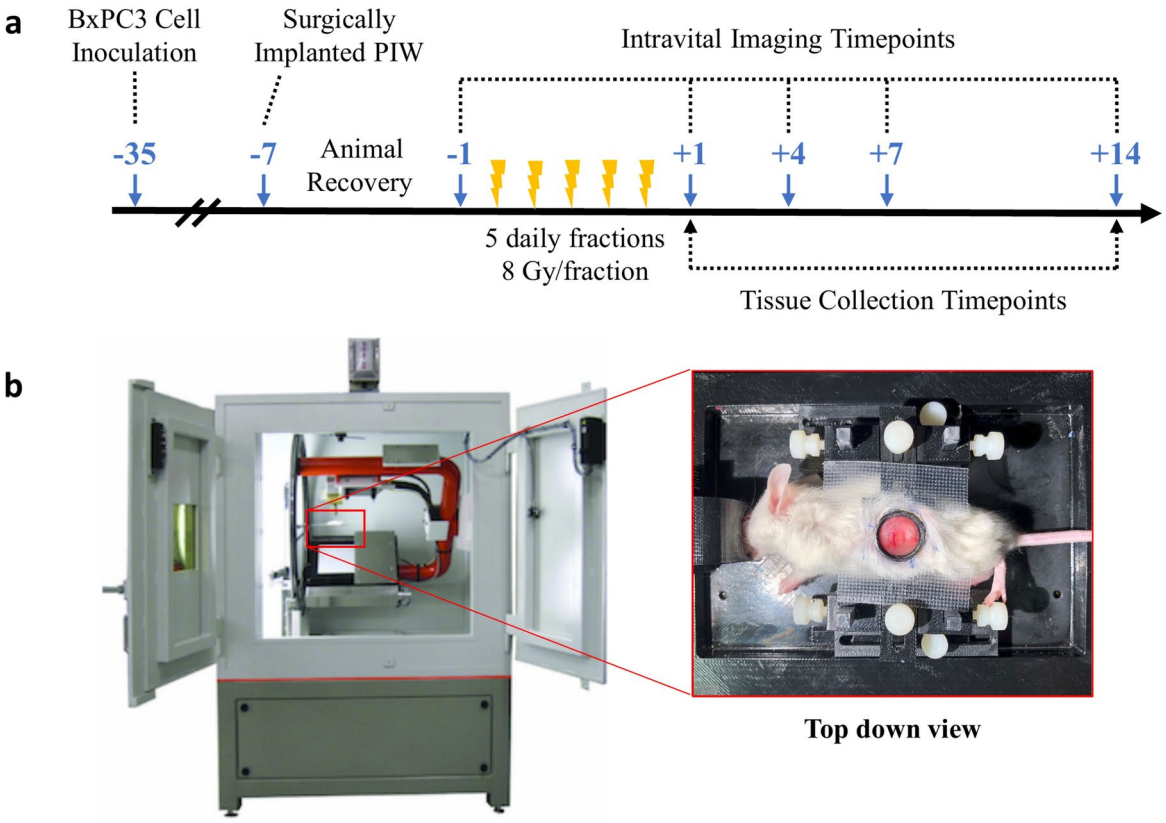

Fig. 2. Experiment design. (**a**) Schematic timeline of BxPC3 cell inoculation, surgical implantation of pancreatic imaging window (PIW), SBRT treatment, and schedule for serial intravital imaging. Blue arrows indicate the number of days before (−) and after (+) SBRT treatment. Intravital imaging was performed 1 day before and 1, 4, 7 and 14 days post-SBRT. Mice were euthanized at days +1 and +14 for tissue collection and immunohistochemical (IHC) staining. (**b**) SBRT given in 5 daily fractions of 8 Gy (5 × 8 Gy) using an X-Rad 225Cx micro-irradiator. Inset image shows the mouse positioned on its right flank on a custom, 3D-printed stage (also pictured in Fig. 1E). The custom stage minimizes motion artifacts and ensures that the irradiated and imaging regions are identical.

tumor cell proliferation and tumor cell density within the irradiated pancreas in the SBRT group, compared with non-irradiated tumors. The total area of tumor microvasculature was also found to decrease 1 day after SBRT.

While this study is primarily a technical demonstration in the preclinical setting, our findings highlight the potential for SBRT not only to reduce tumor cell proliferation but also to modify the vasculature and hypoxic status of the pancreatic TME in a time-dependent manner. Further research with larger cohorts is needed to confirm these biological effects and strengthen the applicability of the findings. Future studies using our intravital optical imaging platform can continue to explore how these SBRT-induced changes to the pancreatic TME occur in a dose-dependent manner and investigate new ways to optimize dose and fractionation schemes to improve the effectiveness of clinical SBRT of pancreatic cancer patients.

Results

SBRT decreases BxPC3-DsRed tumor cell fluorescence and proliferation

The primary goal of cancer radiotherapy is to kill malignant cells and control tumor growth. To confirm that SBRT was indeed targeting BxPC3 tumor cells in our study, we used both IVFM (Fig. 3) and IHC staining to monitor orthotopic tumors in vivo for up to two weeks after SBRT. The mean fluorescence intensity (MFI) of DsRed in BxPC3 cells was found to decrease in the SBRT group, reaching statistical significance 7 days after treatment (0.75 vs. 1.39-fold change relative to day −1 DsRed MFI, $p < 0.05$, Fig. 4a). IHC staining of BxPC3 tumor sections were found to have significantly increased γH2AX staining (DNA damage) 1 day post-SBRT compared to non-irradiated tumors (50% vs. 6%, $p < 0.05$), with a reduction to values similar to non-irradiated tumors at the 14-day time point (3% vs. 1%, $p = 0.15$, Fig. 4b,c). Tumor sections treated with SBRT showed decreased Ki67 staining (tumor cell proliferation) 1 day post-SBRT (1% vs. 6%, $p = 0.09$), which reached statistical significance 14 days post-SBRT compared to non-irradiated tumors (1% vs 7%, $p < 0.001$, Fig. 4d,e).

SBRT decreases tumor hypoxia

To understand the effect of SBRT on BxPC3 tumor cell hypoxia in vivo, IVFM was used to measure BxPC3 cell 5xHRE/GFP fluorescence intensity for up to two weeks after SBRT. The GFP MFI in BxPC3 cells was found

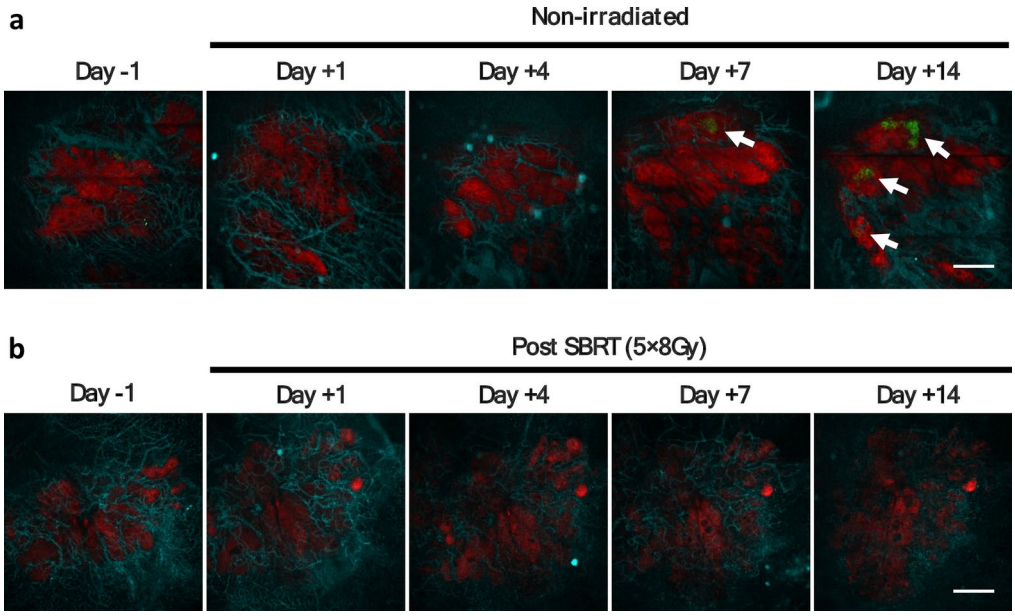

Fig. 3. Intravital fluorescence microscopy (IVFM) enables longitudinal monitoring of orthotopic BxPC3 tumors in vivo. Top row (**a**) shows representative fluorescence images of non-irradiated BxPC3 tumors in one mouse. Bottom row (**b**) shows representative fluorescence images of BxPC3 tumors treated with 5 × 8 Gy SBRT in another mouse. BxPC3 cells (DsRed) are shown in red and tumor cell HIF activity (5xHRE/GFP) in green. White arrows indicate regions of BxPC3 tumor cell HIF activity. In vivo labeling of tumor microvasculature was performed by intravenous injection of APC-conjugated CD31 antibody (cyan). Scale bar = 500 µm.

to decrease in the SBRT group one day after treatment (0.62 vs. 1.28-fold change relative to day −1 GFP MFI, $p < 0.05$, Fig. 5a) and all subsequent days, albeit not significantly. Tumors stained for carbonic anhydrase IX (CA9), a marker of tumor hypoxia, showed significantly decreased staining at both 1 and 14 days post-SBRT, compared to non-irradiated tumors ($p < 0.05$, Fig. 5b,c).

SBRT decreases tumor cell density

In general, one of the main factors contributing to tumor hypoxia is the rapid proliferation of malignant cells beyond their vascular supply of oxygen[41]. To investigate whether the density of pancreatic tumor cells may have played a role in the development of hypoxia in vivo, we analyzed cell density using H&E-stained tissue sections of BxPC3 tumors. This revealed an average decrease of 22% in tumor cell density 1 day post-SBRT compared with non-irradiated BxPC3 tumors ($p < 0.01$, Fig. 6). There were no significant differences between groups in BxPC3 tumor cell density 14 days post-SBRT ($p = 0.30$).

SBRT decreases total tumor vascular area

Blood vessels are the main source of oxygen in nearly all tissues, especially tumors. To investigate the effect of SBRT on tumor vasculature, we used both IVFM and IHC staining to monitor orthotopic tumors in vivo for up to two weeks after SBRT. For IVFM, APC-conjugated anti-CD31 antibody was injected intravenously immediately before each in vivo imaging session. Intravital imaging results showed no significant differences in blood vessel density (relative to day −1) between SBRT-treated and non-irradiated groups at any of the imaging timepoints (Fig. 7a). However, blood vessel density in both groups show a decreasing trend over time. In addition, IHC staining of ex vivo tumor tissue sections with anti-CD31 antibody (endothelial cells) showed no significant difference in endothelial cell density between groups (Fig. 7b,c). Interestingly, the total luminal area of blood vessels in each anti-CD31-stained tumor section showed a 52% decrease in blood vessel area 1 day post-SBRT, compared to non-irradiated tumors ($p < 0.01$, Fig. 7d). There were no significant differences in blood vessel area 14 days post-SBRT ($p = 0.34$).

Discussion

Recent advances in clinical image guidance have enabled techniques like SBRT to deliver large doses of ionizing radiation to pancreatic tumors, while minimizing damage to healthy tissues. Despite its clear benefits, the ultimate success of SBRT in clinical trials for pancreatic cancer has been suboptimal[42]. While several studies have shown that SBRT improves overall survival for pancreatic cancer patients[4–6], treatment failure remains a significant issue[17]. One potential explanation for treatment failure following SBRT is the presence of hypoxia within the pancreatic TME[43]. Tumor hypoxia is known to contribute to treatment resistance to both chemo- and radiotherapy[44,45] and pancreatic tumors have been shown to exhibit significant levels of inherent hypoxia[46]. In addition, hypoxia has been shown to predict more aggressive growth and spontaneous metastasis formation in pancreatic tumor models[47]. Thus, understanding the radiobiological response of pancreatic tumors to SBRT,

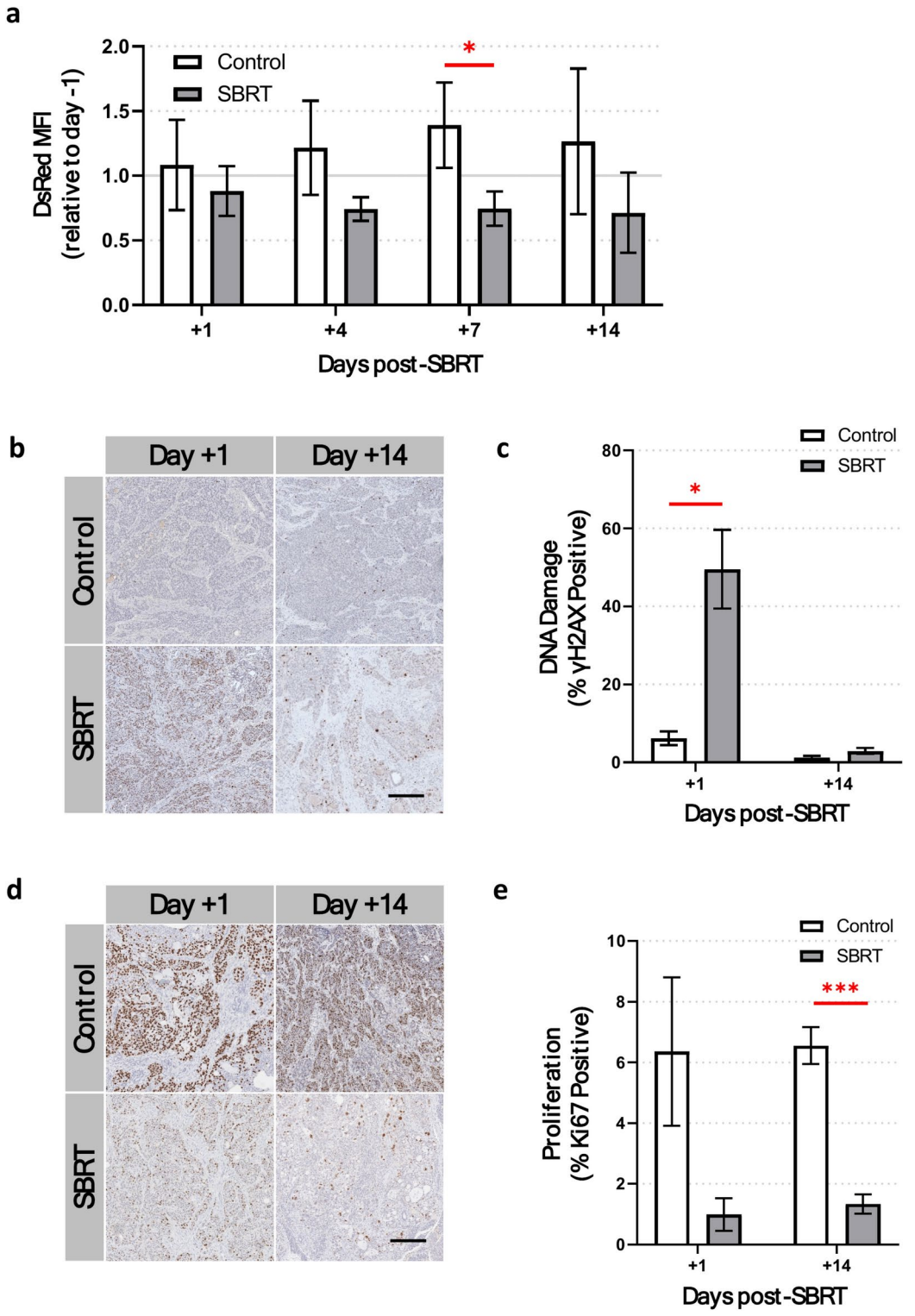

Fig. 4.. 5×8 Gy SBRT decreases pancreatic tumor cell proliferation. (**a**) Intravital fluorescence microscopy reveals a persistent decrease in the DsRed mean fluorescence intensity (MFI) of DsRed-BxPC3 tumor cells up to 14 days post-SBRT (grey bars) compared to non-irradiated BxPC3 tumor cells (white bars). (**b**) Representative images and (**c**) quantification of γH2AX staining (brown) in ex vivo BxPC3 tumor tissue sections show significant DNA damage in tumor cells 1 day post-SBRT, compared to non-irradiated control mice. No significant differences in γH2AX staining are seen 14 days after treatment. (**d**) Representative images and (**e**) quantification of Ki67 expression (brown) shows a significant decrease in tumor cell proliferation 14 days post-SBRT, compared to non-irradiated animals. Tissue sections are counterstained with hematoxylin (blue). Scale bar = 200 µm. n = 7 mice per group. *$p < 0.05$, **$p < 0.01$, ***$p < 0.001$.

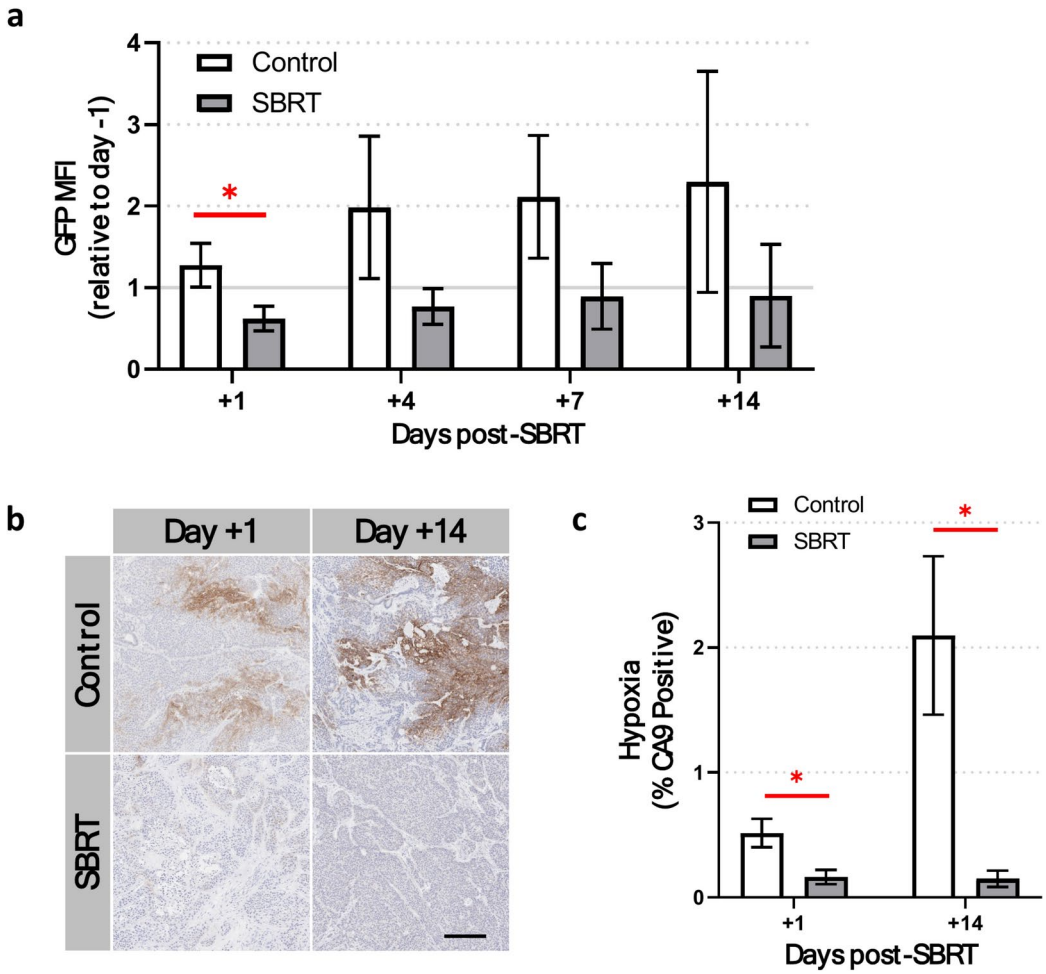

Fig. 5.. 5 × 8 Gy SBRT decreases pancreatic tumor hypoxia. (**a**) Intravital fluorescence microscopy of 5xHRE/GFP-expressing BxPC3 tumor cells show a significant decrease in the GFP mean fluorescence intensity (MFI) 1 day post-SBRT. (**b**) Representative images and (**c**) quantification of CA9 staining (brown) in ex vivo BxPC3 tumor tissue sections show a significant decrease in tumor cell hypoxia at both 1 and 14 days post-SBRT, compared to non-irradiated control mice. Tissue sections are counterstained with hematoxylin (blue). Scale bar = 200 μm. n = 7 mice per group. *$p < 0.05$.

including its effects on tumor hypoxia within the TME, can help optimize SBRT and improve overall treatment response. In this study, we combined an orthotopic mouse model of pancreatic cancer with an IVFM platform to directly monitor the effects of 5 × 8 Gy SBRT on the pancreatic tumor and TME in vivo. Using this technique, we were able to simultaneously image DsRed fluorescent human pancreatic cancer cells, tumor cell hypoxia (using a 5xHRE/GFP reporter), and tumor microvasculature before and (1, 4, 7, and 14 days) after SBRT. Ex vivo IHC staining was performed on excised tumors 1 and 14 days after SBRT to validate in vivo findings.

It is well established that DNA damage is the primary mechanism by which radiotherapy kills tumor cells[48]. In our study, we used IHC staining on tumor tissue sections to quantify significant DNA damage in treated tumors 1 day post-SBRT (Fig. 4b,c), confirming the accurate delivery and treatment effect of ionizing radiation in our orthotopic tumor model. Then, using our mouse intravital imaging platform, we were able to directly monitor the effects of SBRT in orthotopically grown BxPC3-DsRed tumor cells in vivo before and up to two weeks after SBRT. Previous research has demonstrated that constitutively expressed fluorescent proteins are suitable for monitoring total gene expression in cells[49] and overall cell viability[50]. However, it is important to consider that the MFI of DsRed can be influenced by both the fluorescence intensity per tumor cell (cellular viability) and the number of fluorescent tumor cells per unit area (cellularity). In our experiment, we found that the DsRed MFI persistently decreased for up to two weeks post-SBRT, compared to non-irradiated tumors (Fig. 4a). This decrease in DsRed MFI was further supported by a decrease in tumor cell proliferation (Ki67 expression) post-SBRT (Fig. 4d,e). These results are consistent with clinical studies showing decreased Ki67 expression in pancreatic tumors following SBRT[51], which is associated with progression-free survival[52]. Overall, our experiment demonstrated a marked treatment response in orthotopic BxPC3 tumors following SBRT, resulting in both DNA damage and decreased cellular activity (i.e., viability and proliferation), compared with non-irradiated tumors.

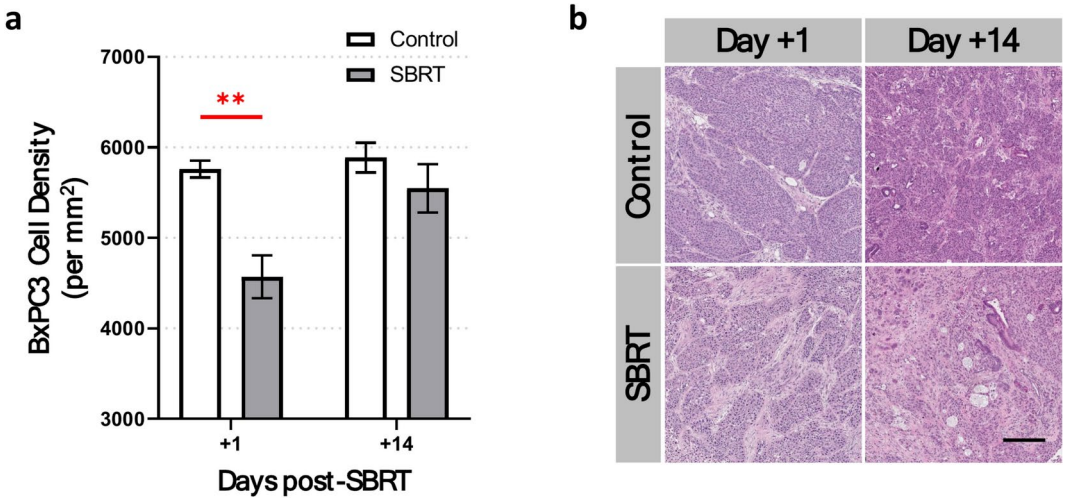

Fig. 6. 5×8 Gy SBRT decreases tumor cell density. (**a**) Hematoxylin and eosin (H&E) staining of ex vivo BxPC3 tumor tissue sections show a significant decrease in tumor cell density 1 day post-SBRT compared with non-irradiated tumors. No significant differences are seen in tumor cell density between irradiated and non-irradiated tumors at 14 days post-SBRT. (**b**) Representative images show H&E-stained BxPC3 tumor sections. Scale bar = 200 μm. n = 7 mice per group. *$p < 0.05$, **$p < 0.01$.

Hypoxia is also an important component of the TME[53]. It is a major contributor to treatment resistance in pancreatic tumors[45] and also promotes a more invasive and malignant phenotype[54]. In this study, we demonstrate that 5×8 Gy SBRT significantly decreased tumor hypoxia in our orthotopic pancreatic tumor model within the first 2 weeks after treatment completion. Using IVFM to monitor HRE-driven GFP fluorescence (a biomarker of tumor hypoxia in BxPC3 tumors[39]) we found that the GFP MFI decreased as early as 1 day after SBRT, compared to non-irradiated tumors (Fig. 5a). To corroborate these observations, IHC staining of BxPC3 tumors showed a significant decrease in CA9 expression at both 1 and 14 days after SBRT, compared to non-irradiated tumors (Fig. 5b,c). CA9 is another biomarker of hypoxia and has previously been used to assess hypoxic fraction in tumors[55,56]. While the in vivo GFP MFI was not statistically significant between experimental groups 14 days after SBRT ($p = 0.30$), our previous research[57] demonstrated that in vivo 5xHRE/GFP fluorescence intensity is directly correlated with ex vivo CA9 expression in our tumor model. Thus, the discrepancy in our results at day 14 could be due to various factors. For instance, although IVFM provides the advantage of longitudinally evaluating fluorescent biomarkers in vivo in the same animal—in this case, for monitoring tumor cell hypoxia—the direct nature of this imaging technique (i.e., directly imaging HRE-driven tumor cell GFP expression) does not offer the same level of signal amplification as secondary antibody labeling methods would. Consequently, IVFM may be less sensitive at detecting subtle changes in tumor cell hypoxia compared with ex vivo tissue-based antibody-labeling methods (e.g., IHC). Nevertheless, previous work has shown a strong relationship between tumor cell HRE-driven based GFP fluorescence intensity and GFP protein expression detected using Western blot[57]. Hence, despite the discrepancy between IVFM and ex vivo tissue IHC in this experiment, we can conclude that 5×8 Gy SBRT produced a reoxygenation effect as early as 1 day post-SBRT in our pancreatic tumor model, which persisted for at least 14 days following SBRT.

Reoxygenation is one of the 'four Rs' of conventional radiotherapy[30]. As ionizing radiation kills tumor cells, it allows more oxygen to reach previously hypoxic cells, reoxygenating the tumor for additional fractions of radiotherapy[58]. However, studies using higher doses of radiotherapy (e.g., SBRT) have sometimes produced the opposite effect, causing acute radiation-induced vascular damage and *increased* tumor hypoxia[24,27,28,59]. Other preclinical studies of SBRT have produced similar results to our own, showing *decreased* tumor hypoxia, either by conventional reoxygenation of the tumor or by promoting improved blood vessel perfusion[43,60–62]. The varying effects of SBRT on tumor oxygenation are likely dependent on the total radiation dose and fractionation schedule as well as tumor model, type, site, and stage[63]. Nevertheless, this inconsistency in the literature requires a better understanding of the radiobiological mechanisms impacting tumor (re)oxygenation following SBRT. Optimizing SBRT to reoxygenate the pancreatic TME may help prevent occurrences of spontaneous metastasis and relapse following SBRT, improving treatment outcomes.

Tumor oxygenation is controlled by two main factors: the *demand* for oxygen from proliferating tumor cells and the *supply* of oxygen from (tumor) blood vessels[64]. Decreased oxygen consumption within a tumor, either from decreased tumor cell density or decreased cell metabolic activity, can improve tumor oxygenation[65]. Conversely, improving the functionality of tumor microvasculature can increase blood perfusion and oxygen delivery to tumor tissue[66]. To better understand the underlying cause of reoxygenation in our pancreatic tumor model following SBRT, we examined whether changes in oxygenation were caused by either a decrease in oxygen demand or an increase in oxygen supply (or both).

In general, tissue oxygen concentrations are inversely proportional to cell density[67]. Once cells lose their contact inhibition (a key step in malignant transformation) and experience uncontrolled proliferation, the

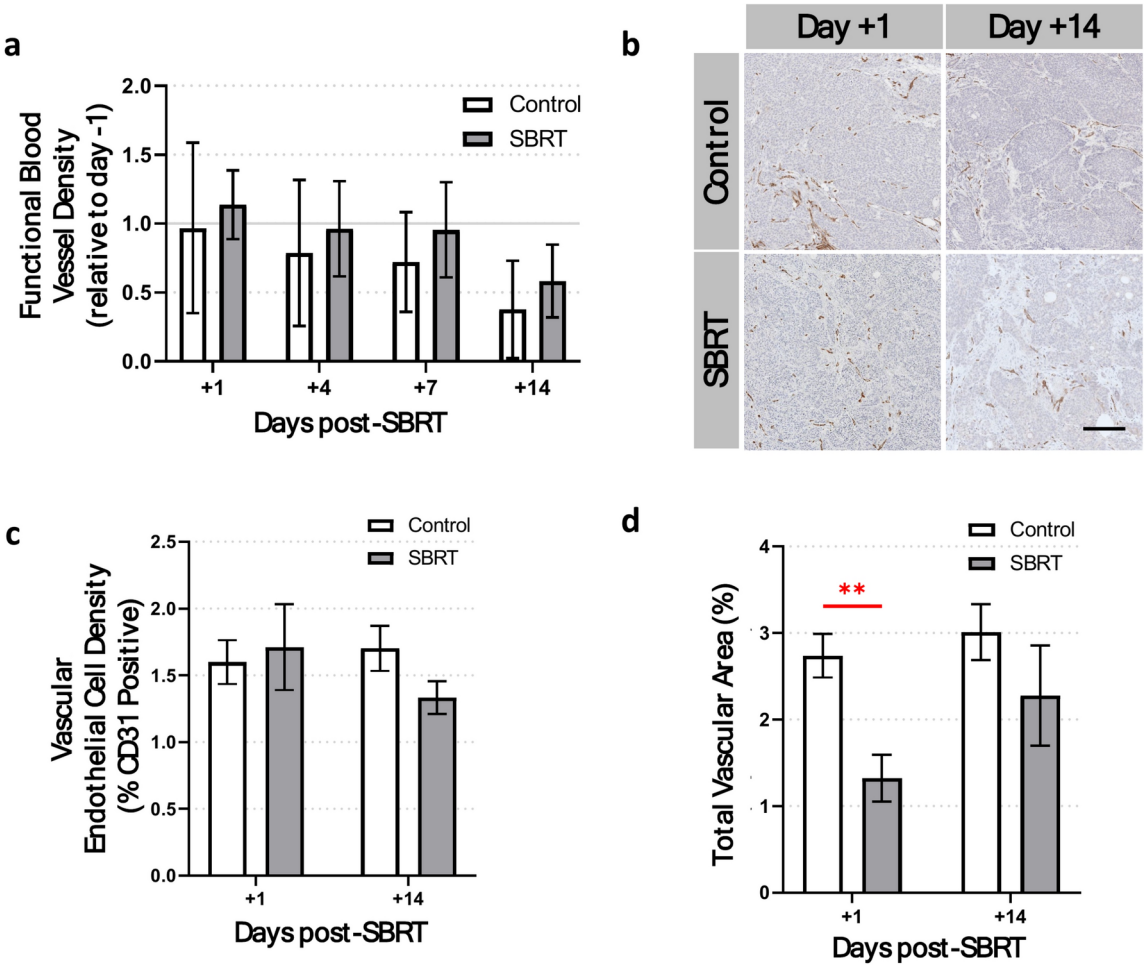

Fig. 7. Effect of SBRT on tumor blood vessels. (**a**) Intravital fluorescence microscopy of BxPC3 tumor blood vessels (stained in vivo with APC-CD31) shows no significant change in functional blood vessel density between groups. (**b**) Representative images and (**c**) quantification of CD31 expression in ex vivo BxPC3 tumor tissue sections show no significant differences in vascular endothelial cell density between groups. Tissue sections are counterstained with hematoxylin (blue). (**d**) Total vascular area (%) shows a significant decrease 1 day post-SBRT. No significant differences in vascular area staining are seen 14 days after treatment. n = 7 mice per group. $^{**}p < 0.01$.

physical constraints of the surrounding tissue can lead to overcrowding of cells[68]. This increasing density of tumor cells has been shown to limit the penetration of anticancer drugs[69] and increase local O_2 consumption leading to localized regions of hypoxia[70] and upregulation of HIF activity as well as other hypoxia response pathways. In our experiment, we used hematoxylin and eosin (H&E) staining to show that tumor cell density decreased significantly by an average of 22% in tumors 1-day post-SBRT, compared to non-irradiated tumors (Fig. 6). This dramatic decrease in cell density may have reduced O_2 demand within the tumors, explaining the corresponding decrease in tumor hypoxia 1 day post-SBRT. However, given that the difference in cell density was not statistically significant 14 days after SBRT, despite a persistent decrease in CA9 expression (Fig. 5b), it is likely that other factors contributed to the sustained reoxygenation of the tumor at later time points. For example, cellular proliferation (Ki67 expression) and viability (DsRed fluorescence) were both significantly decreased at 7 and 14 days post-SBRT, respectively. Cellular proliferation and metabolic activity have previously been shown to have a direct impact on oxygen consumption rates in tumor cells[71]. Thus, our results suggest that the observed reoxygenation of tumors following SBRT in our study was likely driven by a decrease in oxygen *demand* within the tumor tissue.

A functional vascular network is essential to supply oxygen to the pancreatic TME[72]. Pancreatic tumors with a high microvascular density (MVD) tend to be less hypoxic than those with low MVD[73]. Indeed, we have demonstrated this relationship using our intravital animal model in a previous study[39]. Thus, to understand how pancreatic tumor microvasculature responded to SBRT (and potentially influenced tumor hypoxia), we analyzed the blood vessel density of tumors using both in vivo IVFM (Fig. 7a) and ex vivo IHC staining of CD31-positive vascular endothelial cells (Fig. 7b,c). From both data, no significant differences in blood vessel density were observed between SBRT-treated and non-irradiated tumors at any of our imaging timepoints. Interestingly, our group[74] and others[24,75] have previously shown that high doses of radiotherapy—typically

greater than 10 Gy per fraction[63]—can cause severe vascular damage in tumors. Thus, it is likely that the dosing schedule in our experiment (5 daily fractions of 8 Gy) was below the threshold to inflict significant vascular damage. Conversely, other studies have shown that using similar doses of radiotherapy can potentially *improve* tumor vasculature function through multiple mechanisms. For example, Sonveaux et al.[62] found that irradiating hepatocarcinoma xenografts with 1 × 6 Gy increases tumor blood flow and oxygenation through a vascular nitric oxide (NO)-dependent pathway. Tong et al.[61] also found that irradiating non-small cell lung cancer xenografts with 1 × 12 Gy resulted in a brief window of 'vascular normalization' and subsequent reoxygenation 7- and 14-days post-radiotherapy. This effect coincided with a downregulation of the p-STAT3/HIF-1α pathway (as well as its downstream angiogenic factors: VEGFA and CXCL12), resulting in decreased tumor blood vessel diameter and tortuosity, and increased pericyte coverage. In our experiment, we were able to observe a similar phenomenon in CD31-stained tumor tissue sections with a significant decrease in total vascular area 1 day post-SBRT (Fig. 7d). Given that tumor microvasculature is often pathologically dilated and irregular in size[76,77], a transient decrease in tumor vascular area following 5 × 8 Gy SBRT may suggest that there was a brief window of vascular normalization. However, future studies are needed to validate whether this phenomenon occurred and if it played a significant role in the reoxygenation of our pancreatic tumor model after SBRT.

In summary, by combining in vivo IVFM and ex vivo IHC staining, we were able to validate our dually fluorescent pancreatic tumor cell line to simultaneously monitor tumor response to SBRT in vivo and assess tumor cell hypoxia in an orthotopic mouse model of pancreatic cancer. Preliminary biological findings using this model demonstrated that 5 × 8 Gy SBRT significantly decreased tumor cell viability, proliferation, density, and notably, hypoxia in our pancreatic tumor model. Hypoxia is a major contributor to treatment resistance in pancreatic tumors[45] and promotes a more invasive and malignant phenotype[54]. Thus, understanding the extent (and time course) of tumor reoxygenation following SBRT can help optimize radiation dose and fractionation schemes in the clinical setting and improve treatment response. While our intravital imaging platform allowed us to monitor the short-term effects (days to weeks) of SBRT on the pancreatic TME, follow-up studies are needed to appreciate the long-term impact of these changes on tumor control, metastasis, and overall survival.

While these findings offer valuable insights into the response of BxPC3 tumors to 5 × 8 Gy SBRT, it is important to consider limitations in the experimental approach used in this study when interpreting our findings. One potential limitation of this study is the relatively low number of mice used as experimental subjects, which may have hindered our ability to detect statistically significant differences between different experimental groups. Second, while we decided to control for potential gender-related variability in our experimental results by only using female mice, there is increasing evidence of sexual dimorphism in treatment response in several tumor types, including pancreatic tumors[78]. Therefore, caution should be exercised when generalizing the findings of this study to male mice or human populations. Future studies incorporating both male and female subjects are needed to comprehensively understand the effects of the intervention between sexes and improve the overall validity and generalizability of these findings. Third, while cell line–derived tumor models, such as the one used in this study, are ideal for intravital imaging experiments due to their consistent and predictable tumor growth kinetics, they are limited in their ability to study the TME due to their immunodeficient murine host system. Thus, future work is encouraged to corroborate these findings in immunocompetent murine model systems (e.g., genetically engineered mouse models, or GEMMs) that can better recapitulate the pancreatic TME in human disease. This could substantially enhance the translational impact of such research. As previously mentioned, the effects of SBRT on solid tumors are likely dependent on several factors, including treatment regimen, tumor type, site, and stage[63]. Future work can continue to explore how SBRT-induced reoxygenation occurs in a dose-dependent manner, and if this effect is generalizable to other pancreatic tumor models, in order to better predict treatment response.

Methods

Cell line

Fluorescently labeled BxPC3-DsRed human pancreatic adenocarcinoma cells[79] (AntiCancer, San Diego, CA, USA) were grown in RPMI 1640 medium supplemented with 2 mM L-glutamine, 10% fetal bovine serum, and 1% penicillin–streptomycin at 37.0 °C and 5% CO_2. To report on tumor cell hypoxia-inducible factor (HIF) activity, BxPC3 cells were stably transfected with a 5× Hypoxia Response Element-GFP construct ('5xHRE/GFP', a gift from Martin Brown and Thomas Foster, Addgene plasmid #46926), as previously described[80]. The GFP expression of this modified cell line, hereinafter referred to as BxPC3-DsRed-5xHRE/GFP, was characterized in a previous publication by our group[39].

Mouse model and pancreatic imaging window surgery

All animal experiments were conducted in accordance with regulatory standards approved by the University Health Network Animal Care Committee (Animal Use Protocol #2613) and reported in compliance with the ARRIVE guidelines.

Orthotopic BxPC3-DsRed-5xHRE/GFP pancreatic tumors were established in 8- to 10-week-old female NRG mice (Jackson Laboratory, #007799) as previously described[81]. Briefly, anesthetized animals were administered 0.1 mg/kg of buprenorphine and maintained under isoflurane in oxygen (5% induction, 2% maintenance) in a right-lateral position on a heated pad. Fur on the left-lateral side was removed, and the surgical site was sterilized with iso-betadine and ethanol solutions. A 1 cm paramedian incision was made, penetrating the skin and peritoneum between the spleen and spine. The head of the pancreas was then carefully exteriorized, rinsed with saline, and inoculated with 1×10^6 BxPC3-DsRed-5xHRE/GFP cells suspended in 10 µl of phosphate-buffered saline mixed with 10 µl of Matrigel (Corning Inc., Corning, NY) using a 29G insulin syringe (Becton Dickinson, Franklin Lakes, NJ). After slow retraction of the needle, a sterile cotton swab was applied over the puncture site for 60 s to prevent fluid backflow. Subsequently, the pancreas was gently returned to the abdominal cavity,

and the peritoneum and skin were closed using 4.0 absorbable sutures (Ethicon, Somerville, NJ) and surgical staples, respectively. Tumor growth was monitored weekly through ultrasound imaging (Vevo 2100; FUJIFILM VisualSonics Inc., Toronto, Canada) to assess tumor progression.

Once tumors reached ~ 5 mm in diameter (5 weeks post-inoculation), a custom-designed pancreatic imaging window (PIW), with an inner diameter of 12 mm, a thickness of 1.8 mm and 8 equally spaced 1 mm holes (Fig. 1a,b) was 3D-printed with biocompatible, acrylonitrile butadiene styrene (ABS) plastic and surgically implanted over the tumor site (Fig. 1c). The surgical procedure for PIW implantation was performed as previously described[39].

Intravital fluorescence microscopy (IVFM)

After one week of recovery from PIW implantation, serial IVFM of pancreatic tumors was performed using an LSM710 laser-scanning confocal microscope (Carl Zeiss Canada, Ltd., Fig. 1d). To facilitate live-animal imaging on the microscope and obtain consistent high-quality images, a custom-designed, 3D-printed microscope stage insert (made with ABS) was used with a built-in isoflurane port to maintain anesthesia during imaging, an electrical heating pad was embedded in the stage in order to maintain physiological body temperature of the animal, and a PIW holder was used to reduce motion artifacts during imaging (Fig. 1e). All animals were anesthetized using isoflurane in oxygen (5% induction, 2% maintenance) and kept at 37 °C throughout each imaging session. Tumor blood vessels were fluorescently labeled by intravenous injection of APC-conjugated rat anti-mouse CD31 antibody (6 µg, see Table 1) through the tail vein, immediately before each imaging session. 488 nm and 633 nm lasers were used to excite GFP/DsRed and APC, respectively. Intravital imaging sessions typically lasted 15–20 min for each mouse. Images were obtained from 5–10 unique fields of view (FOVs) of the pancreatic tumor using a 5×/0.25 NA lens (FOV = 2429 × 2429 µm^2). Figure 2A shows a schematic timeline of all intravital imaging time points.

Radiation treatment

To perform SBRT, mice were anesthetized under 2% isoflurane in oxygen and positioned on their right-lateral side using a custom-designed, 3D-printed bed (Fig. 2b). The bed was placed inside an X-RAD 225Cx small animal irradiator (Precision X-ray, Inc., North Branford, CT) and a cone-beam computed tomography (CBCT) scan was acquired to visualize the anatomy of the mouse. The three-axis translation stage was repositioned to target the tumor directly below the imaging window. A treatment plan (previously calculated in SmART-Plan, Precision X-ray, Inc.) was delivered using a 1 cm diameter circular collimator. Two opposing beams from above and below the animal (4 Gy/beam) were used to create a uniform dose distribution across the tumor, administered at a dose rate of 2.55 Gy/min. This treatment was repeated over 5 consecutive days (8 Gy per treatment fraction) for a total dose of 40 Gy. In our experimental setup, dosimetry and dose delivery schedules for all irradiation experiments were overseen by a clinical medical physicist. Moreover, the well-being of the mice was closely monitored by veterinary technicians during and after SBRT. No signs of adverse effects from treatment (e.g., weight loss, pain, diarrhea) were observed.

Intravital image analysis

All IVFM (in vivo) images were analyzed using a custom MATLAB script (vR2021A, The MathWorks, Inc.). Before quantification, linear unmixing of all spectral image data was performed using an algorithm previously described by T. Zimmerman[82]. Briefly, a coefficient matrix (***R***) was first created using control samples of each fluorophore to measure their relative contribution to each channel. Then, the measured signal intensity in each channel (***S***) was used to determine the amount of each fluorophore (***A***) by solving matrix Eq. (1).

$$S = A \times R \tag{1}$$

To quantify 5xHRE/GFP and DsRed fluorescence intensity in BxPC3 cells in vivo, a binary image was first created using DsRed fluorescence intensity to identify the tumor cell region of interest ('Tumor ROI'). The threshold for DsRed fluorescence intensity was empirically determined to be above background fluorescence. Mean tumor cell GFP fluorescence intensity (GFP MFI) was calculated as the sum of each pixel's GFP fluorescence intensity within the Tumor ROI divided by the number of pixels in the Tumor ROI. Mean tumor cell DsRed fluorescence intensity (DsRed MFI) was calculated as the sum of each pixel's DsRed fluorescence intensity within the Tumor ROI divided by the number of pixels in the Tumor ROI.

To quantify tumor vasculature, the Tumor ROI binary image was morphologically dilated by 100 µm beyond the tumor boundary (creating a 'Expanded Tumor ROI') to account for blood vessels along the tumor periphery (and within the nominal diffusion limit of O_2 in tissues[83]). Blood vessels were segmented from APC-

	Primary antibody	Company, catalog #	Dilution	Secondary antibody/reagent	Company, catalog #	Dilution
IVFM	APC-conjugated anti-CD31	BD Biosciences, 551262	0.03 mg/mL	N/A		
IHC	Anti-H2AX	EMD Millipore, 05-636	1:3000	Anti-Mouse IgG	IHC	Anti-H2AX
	Anti-Ki67	Abcam, ab15580	1:1500	Anti-Rabbit IgG	Thermo Fisher Scientific, A-21428	Anti-Ki67
	Anti-CA9	Novus Biologicals, NB100-479	1:50	Anti-Rabbit IgG	Thermo Fisher Scientific, A-21428	Anti-CA9
	Anti-CD31	Abcam, ab182981	1:1000	Anti-Rabbit IgG	Thermo Fisher Scientific, A-21428	Anti-CD31

Table 1. Antibodies and dilutions used in the study.

CD31 fluorescence intensity by performing simple linear iterative clustering (SLIC)[84] followed by adaptive thresholding[85]. Tumor vascular density was calculated as the number of APC-positive pixels within the Expanded Tumor ROI divided by the total number of pixels in the Expanded Tumor ROI.

Immunohistochemical (IHC) staining and analysis

Immediately after the first or final IVFM imaging sessions post-SBRT (day +1 or +14, respectively, Fig. 2a), mice were euthanized and whole tumors were excised from the pancreas, grossly bisected, and laid flat in a cassette which was then fixed in 10% formalin for 48 h and embedded in paraffin. From the centre of the tumor, consecutive 5 µm-thick sections were cut and immunohistochemically stained according to manufacturer's instructions for hematoxylin and eosin (H&E) and biomarkers of DNA damage (γH2AX)[86], tumor cell proliferation (Ki67)[87], tumor cell hypoxia (CA9)[55], and blood vessels (CD31). See Table 1 for antibodies and dilutions used. All slides were scanned at 20× magnification and digitalized using a whole-slide scanner (Aperio Scanscope XT; Aperio Technologies Inc., Vista, CA, USA) and uploaded into the HALO Image Analysis software (v3.3.2541.301, Indica Labs). The HALO Classifier module was used to classify and calculate the viable carcinoma tissue area in sections annotated to only include stained tissue in the analysis. Next, the Area Quantification module was used on the annotated, classified tissue to identify positive staining of each stain and quantify the percentage of positive stain as a ratio of the positive staining area divided by total viable carcinoma tissue area × 100%.

Statistical analysis

All statistical analyses were performed using GraphPad Prism v9.3.1. For intravital imaging, a repeated-measures analysis of variance (ANOVA) followed by Dunnett's multiple comparisons test was performed to compare groups at each time point. Comparisons between two groups were performed using an unpaired Welch's *t*-test. All data are represented as mean ± standard error of the mean (SEM), unless otherwise specified, with significance determined at $p < 0.05$.

Received: 11 September 2023; Accepted: 9 December 2024
Published online: 28 December 2024

References

1. Huang, L. et al. Stratified survival of resected and overall pancreatic cancer patients in Europe and the USA in the early twenty-first century: a large, international population-based study. *BMC Med.* **16** (2018).
2. Surveillance Research Program, N. C. Institute. SEER*Explorer: An interactive website for SEER cancer statistics. https://seer.cancer.gov/statistics-network/explorer/
3. Wolfgang, C. L. et al. Recent progress in pancreatic cancer. *CA Cancer J. Clin.* **63**, 228–230 (2013).
4. de Geus, S. W. L. et al. Stereotactic body radiotherapy for unresected pancreatic cancer: A nationwide review. *Cancer* **123**, 4158–4167 (2017).
5. Zhong, J. et al. Outcomes for patients with locally advanced pancreatic adenocarcinoma treated with stereotactic body radiation therapy versus conventionally fractionated radiation. *Cancer* **123**, 3486–3493 (2017).
6. Tchelebi, L. T. et al. Conventionally fractionated radiation therapy versus stereotactic body radiation therapy for locally advanced pancreatic cancer (CRiSP): An international systematic review and meta-analysis. *Cancer* **126**, 2120–2131 (2020).
7. Loehrer, P. J. et al. Gemcitabine alone versus gemcitabine plus radiotherapy in patients with locally advanced pancreatic cancer: an eastern cooperative oncology group trial. *J. Clin. Oncol.* **29**, 4105 (2011).
8. Mahadevan, A. et al. Induction gemcitabine and stereotactic body radiotherapy for locally advanced nonmetastatic pancreas cancer. *Int. J. Radiat. Oncol. Biol. Phys.* **81** (2011).
9. Koong, A. C. et al. Phase I study of stereotactic radiosurgery in patients with locally advanced pancreatic cancer. *Int. J. Radiat. Oncol. Biol. Phys.* **58**, 1017–1021 (2004).
10. Comito, T. et al. Can stereotactic body radiation therapy be a viable and efficient therapeutic option for unresectable locally advanced pancreatic adenocarcinoma? Results of a phase 2 study. *Technol. Cancer Res. Treat.* **16**, 295–301 (2017).
11. Schellenberg, D. et al. Single-fraction stereotactic body radiation therapy and sequential gemcitabine for the treatment of locally advanced pancreatic cancer. *Int. J. Radiat. Oncol. Biol. Phys.* **81**, 181–188 (2011).
12. Herman, J. M. et al. Phase 2 multi-institutional trial evaluating gemcitabine and stereotactic body radiotherapy for patients with locally advanced unresectable pancreatic adenocarcinoma. *Cancer* **121**, 1128–1137 (2015).
13. Polistina, F. et al. Unresectable locally advanced pancreatic cancer: a multimodal treatment using neoadjuvant chemoradiotherapy (gemcitabine plus stereotactic radiosurgery) and subsequent surgical exploration. *Ann. Surg. Oncol.* **17**, 2092–2101 (2010).
14. Hoyer, M. et al. Phase-II study on stereotactic radiotherapy of locally advanced pancreatic carcinoma. *Radiother. Oncol.* **76**, 48–53 (2005).
15. Chang, D. T. et al. Stereotactic radiotherapy for unresectable adenocarcinoma of the pancreas. *Cancer* **115**, 665–672 (2009).
16. Schellenberg, D. et al. Gemcitabine chemotherapy and single-fraction stereotactic body radiotherapy for locally advanced pancreatic cancer. *Int. J. Radiat. Oncol. Biol. Phys.* **72**, 678–686 (2008).
17. Patel, A. K. et al. Patterns of failure after adjuvant stereotactic body radiation therapy for pancreatic cancer with close or positive margins. *Adv. Radiat. Oncol.* **5**, 1197 (2020).
18. Ghaly, M., Gogineni, E. & Saif, M. W. The evolving field of stereotactic body radiation therapy in pancreatic cancer. *Pancreas (Fairfax)* **3**, 9 (2019).
19. Jung, J. et al. Stereotactic body radiation therapy for locally advanced pancreatic cancer. *PLoS One* **14** (2019).
20. Baskar, R., Dai, J., Wenlong, N., Yeo, R. & Yeoh, K. W. Biological response of cancer cells to radiation treatment. *Front. Mol. Biosci.* **1** (2014).
21. Macià i Garau, M. Radiobiology of stereotactic body radiation therapy (SBRT). *Rep. Pract. Oncol. Radiother.* **22**, 86 (2017).
22. Abi Jaoude, J. et al. Stereotactic versus conventional radiation therapy for patients with pancreatic cancer in the modern era. *Adv. Radiat. Oncol.* **6**, 100763 (2021).
23. Brown, J. M., Carlson, D. J. & Brenner, D. J. The tumor radiobiology of SRS and SBRT: are more than the 5 Rs involved?. *Int. J. Radiat. Oncol. Biol. Phys.* **88**, 254–262 (2014).
24. Park, H. J., Griffin, R. J., Hui, S., Levitt, S. H. & Song, C. W. Radiation-induced vascular damage in tumors: implications of vascular damage in ablative hypofractionated radiotherapy (SBRT and SRS). *Radiat. Res.* **177**, 311–327 (2012).
25. Kim, M. S. et al. Radiobiological mechanisms of stereotactic body radiation therapy and stereotactic radiation surgery. *Radiat. Oncol. J.* **33**, 265–275 (2015).

26. Song, C. W. et al. Indirect tumor cell death after high-dose hypofractionated irradiation: implications for stereotactic body radiation therapy and stereotactic radiation surgery. *Int. J. Radiat. Oncol. Biol. Phys.* **93**, 166–172 (2015).
27. Maeda, A. et al. In vivo imaging reveals significant tumor vascular dysfunction and increased tumor hypoxia-inducible factor-1α expression induced by high single-dose irradiation in a pancreatic tumor model. *Int. J. Radiat. Oncol. Biol. Phys.* **97**, 184–194 (2017).
28. Kelada, O. J. et al. High single doses of radiation may induce elevated levels of hypoxia in early-stage non-small cell lung cancer tumors. *Int. J. Radiat. Oncol. Biol. Phys.* **102**, 174–183 (2018).
29. Horsman, M. R., Wouters, B. G., Joiner, M. C. & Overgaard, J. The oxygen effect and fractionated radiotherapy. In *Basic Clinical Radiobiology* (eds. Joiner, M. & van der Kogel, A.) 207–216 (Hodder Arnold, 2009).
30. Withers, H. R. The four R's of radiotherapy. *Adv. Radiat. Biol.* **5**, 241–271 (1975).
31. Tsai, C. S. et al. Macrophages from irradiated tumors express higher levels of iNOS, arginase-I and COX-2, and promote tumor growth. *Int. J. Radiat. Oncol. Biol. Phys.* **68**, 499–507 (2007).
32. Okubo, M. et al. M2-polarized macrophages contribute to neovasculogenesis, leading to relapse of oral cancer following radiation. *Sci. Rep.* *6*, 1–12 (2016).
33. Crittenden, M. R. et al. Expression of NF-κB p50 in tumor stroma limits the control of tumors by radiation therapy. *PLoS One* **7**, e39295 (2012).
34. Leblond, M. M. et al. Hypoxia induces macrophage polarization and re-education toward an M2 phenotype in U87 and U251 glioblastoma models. *Oncoimmunology* **5** (2016).
35. Alieva, M., Ritsma, L., Giedt, R. J., Weissleder, R. & Van Rheenen, J. Imaging windows for long-term intravital imaging: General overview and technical insights. *Intravital* **3** (2014).
36. Tsuzuki, Y. et al. Pancreas microenvironment promotes VEGF expression and tumor growth: novel window models for pancreatic tumor angiogenesis and microcirculation. *Lab. Investig.* **81**, 1439–1451 (2001).
37. Jain, R. K., Munn, L. L. & Fukumura, D. Pancreatic tumor preparation in mice. *Cold Spring Harb. Protoc.* **2012**, 1298–1299 (2012).
38. Ritsma, L. et al. Surgical implantation of an abdominal imaging window for intravital microscopy. *Nat. Protoc.* **8**, 583–594 (2013).
39. Samuel, T. et al. Quantitative intravital imaging for real-time monitoring of pancreatic tumor cell hypoxia and stroma in an orthotopic mouse model. *Sci. Adv.* (2023) **(in press)**.
40. Palta, M. et al. Radiation therapy for pancreatic cancer: executive summary of an ASTRO clinical practice guideline. *Pract. Radiat. Oncol.* **9**, 322–332 (2019).
41. Petrova, V., Annicchiarico-Petruzzelli, M., Melino, G. & Amelio, I. The hypoxic tumour microenvironment. *Oncogenesis* **7**, 1–13 (2018).
42. Hajj, C. & Goodman, K. A. Pancreatic cancer and SBRT: A new potential option?. *Rep. Pract. Oncol. Radiother.* **20**, 377–384 (2015).
43. Taylor, E. et al. Quantifying reoxygenation in pancreatic cancer during stereotactic body radiotherapy. *Sci. Rep.* **10**, 1–13 (2020).
44. Dhani, N., Fyles, A., Hedley, D. & Milosevic, M. The clinical significance of hypoxia in human cancers. *Semin. Nucl. Med.* **45**, 110–121 (2015).
45. Tan, Z. et al. Hypoxia: a barricade to conquer the pancreatic cancer. *Cell. Mol. Life Sci.* **77**, 3077–3083 (2020).
46. Koong, A. C. et al. Pancreatic tumors show high levels of hypoxia. *Int. J. Radiat. Oncol. Biol. Phys.* **48**, 919–922 (2000).
47. Chang, Q., Jurisica, I., Do, T. & Hedley, D. W. Hypoxia predicts aggressive growth and spontaneous metastasis formation from orthotopically grown primary xenografts of human pancreatic cancer. *Cancer Res.* **71**, 3110–3120 (2011).
48. Sia, J., Szmyd, R., Hau, E. & Gee, H. E. Molecular mechanisms of radiation-induced cancer cell death: a primer. *Front. Cell Dev. Biol.* **8**, 41 (2020).
49. Soboleski, M. R., Oaks, J. & Halford, W. P. Green fluorescent protein is a quantitative reporter of gene expression in individual eukaryotic cells. *FASEB J.* **19**, 1–20 (2005).
50. Csepregi, R., Temesfoi, V., Poór, M., Faust, Z. & Koszegi, T. Green fluorescent protein-based viability assay in a multiparametric configuration. *Molecules* **23**, 1575 (2018).
51. Farren, M. R. et al. Immunologic alterations in the pancreatic cancer microenvironment of patients treated with neoadjuvant chemotherapy and radiotherapy. *JCI Insight* **5** (2020).
52. Wang, L. et al. High proliferation is independently associated with disease progression in metastatic pancreatic adenocarcinoma. *Ann. Oncol.* **29**, v10 (2018).
53. Li, Y., Zhao, L. & Li, X. F. Hypoxia and the Tumor Microenvironment. *Technol. Cancer Res. Treat.* **20** (2021).
54. Diaz, B., Yuen, A. & Díaz, B. The impact of hypoxia in pancreatic cancer invasion and metastasis. *Hypoxia* **2** (2014).
55. Švastová, E. et al. Hypoxia activates the capacity of tumor-associated carbonic anhydrase IX to acidify extracellular pH. *FEBS Lett.* **577**, 439–445 (2004).
56. van den Beucken, T. et al. Hypoxia-induced expression of carbonic anhydrase 9 is dependent on the unfolded protein response. *J. Biol. Chem.* **284**, 24204 (2009).
57. Samuel, T. et al. Quantitative intravital imaging for real-time monitoring of pancreatic tumor cell hypoxia and stroma in an orthotopic mouse model. *Sci. Adv.* **9** (2023).
58. Hall, E. J. & Giaccia, A. J. Oxygen effect and reoxygenation. In *Radiobiology for the Radiologist* (Lippincott Williams & Wilkins, 2006).
59. Kioi, M. et al. Inhibition of vasculogenesis, but not angiogenesis, prevents the recurrence of glioblastoma after irradiation in mice. *J. Clin. Investig.* **120**, 694–705 (2010).
60. Crokart, N. et al. Early reoxygenation in tumors after irradiation: determining factors and consequences for radiotherapy regimens using daily multiple fractions. *Int. J. Radiat. Oncol. Biol. Phys.* **63**, 901–910 (2005).
61. Tong, F. et al. Hypo-fractionation radiotherapy normalizes tumor vasculature in non-small cell lung cancer xenografts through the p-STAT3/HIF-1 alpha signaling pathway. *Ther. Adv. Med. Oncol.* **12**, 1758835920965853 (2020).
62. Sonveaux, P. et al. Modulation of the tumor vasculature functionality by ionizing radiation accounts for tumor radiosensitization and promotes gene delivery. *FASEB J.* **16**, 1979–1981 (2002).
63. Arnold, K. M. et al. The impact of radiation on the tumor microenvironment: effect of dose and fractionation schedules. *Cancer Growth Metastasis* **11**, 117906441876163 (2018).
64. Gulledge, C. J. & Dewhirst, M. W. Tumor oxygenation: a matter of supply and demand. *Anticancer Res.* **16**, 741–749 (1996).
65. Chen, Y., Cairns, R., Papandreou, I., Koong, A. & Denko, N. C. Oxygen consumption can regulate the growth of tumors, a new perspective on the Warburg effect. *PLoS One* **4** (2009).
66. Jain, R. K. Antiangiogenesis strategies revisited: from starving tumors to alleviating hypoxia. *Cancer Cell* **26**, 605–622 (2014).
67. Tokyuda, Y., Crane, S., Yamaguchi, Y., Zhou, L. & Falanga, V. The levels and kinetics of oxygen tension detectable at the surface of human dermal fibroblast cultures. *J. Cell Physiol.* **182**, 414–420 (2000).
68. Pavel, M. et al. Contact inhibition controls cell survival and proliferation via YAP/TAZ-autophagy axis. *Nat. Commun.* **9**, 1–18 (2018).
69. Grantab, R., Sivananthan, S. & Tannock, I. F. The penetration of anticancer drugs through tumor tissue as a function of cellular adhesion and packing density of tumor cells. *Cancer Res.* **66**, 1033–1039 (2006).
70. Sheta, E. A., Trout, H., Gildea, J. J., Harding, M. A. & Theodorescu, D. Cell density mediated pericellular hypoxia leads to induction of HIF-1α via nitric oxide and Ras/MAP kinase mediated signaling pathways. *Oncogene* **20**, 7624–7634 (2001).
71. Walenta, S. & Mueller-Klieser, W. Oxygen consumption rate of tumour cells as a function of their proliferative status. *Adv. Exp. Med. Biol.* **215**, 389–391 (1987).

72. Forster, J. C., Harriss-Phillips, W. M., Douglass, M. J. & Bezak, E. A review of the development of tumor vasculature and its effects on the tumor microenvironment. *Hypoxia* **5**, 21 (2017).
73. Gaustad, J. V., Simonsen, T. G., Wegner, C. S. & Rofstad, E. K. Vascularization, oxygenation, and the effect of sunitinib treatment in pancreatic ductal adenocarcinoma xenografts. *Front. Oncol.* **9**, 845 (2019).
74. Maeda, A. et al. In vivo imaging reveals significant tumor vascular dysfunction and increased tumor hypoxia-inducible factor-1α expression induced by high single-dose irradiation in a pancreatic tumor model. *Int. J. Radiat. Oncol. Biol. Phys.* **97**, 184–194 (2017).
75. Demidov, V. et al. Preclinical longitudinal imaging of tumor microvascular radiobiological response with functional optical coherence tomography. *Sci. Rep.* **8**, 1–12 (2018).
76. Jain, R. K. Molecular regulation of vessel maturation. *Nat. Med.* **9**, 685–693 (2003).
77. Forster, J., Harriss-Phillips, W., Douglass, M. & Bezak, E. A review of the development of tumor vasculature and its effects on the tumor microenvironment. *Hypoxia (Auckl)* **5**, 21–32 (2017).
78. He, F., Furones, A. R., Landegren, N., Fuxe, J. & Sarhan, D. Sex dimorphism in the tumor microenvironment—From bench to bedside and back. *Semin. Cancer Biol.* **86**, 166–179 (2022).
79. Tan, M. H. et al. Characterization of a new primary human pancreatic tumor line. *Cancer Investig.* **4**, 15–23 (1986).
80. Vordermark, D., Shibata, T. & Brown, J. M. Green fluorescent protein is a suitable reporter of tumor hypoxia despite an oxygen requirement for chromophore formation. *Neoplasia* **3**, 527–534 (2001).
81. Rapic, S. et al. Assessing the accuracy of bioluminescence image-guided stereotactic body radiation therapy of orthotopic pancreatic tumors using a small animal irradiator. *Radiat. Res.* **197**, 626–637. https://doi.org/10.1667/RADE-21-00161.1197 (2022).
82. Zimmermann, T. Spectral imaging and linear unmixing in light microscopy. *Adv. Biochem. Eng. Biotechnol.* **95**, 245–265 (2005).
83. Baker, A. B. & Farmery, A. D. Inert gas transport in blood and tissues. *Compr. Physiol.* **1**, 569–592 (2011).
84. Achanta, R. et al. SLIC superpixels compared to state-of-the-art superpixel methods. *IEEE Trans. Pattern Anal. Mach. Intell.* **34**, 2274–2281 (2012).
85. Bradley, D. & Roth, G. Adaptive thresholding using the integral image. *J. Graph. GPU Game Tools* **12**, 13–21. https://doi.org/10.1080/2151237X.2007.10129236 (2011).
86. Ivashkevich, A., Redon, C. E., Nakamura, A. J., Martin, R. F. & Martin, O. A. Use of the γ-H2AX assay to monitor DNA damage and repair in translational cancer research. *Cancer Lett.* **327**, 123–133 (2012).
87. Menon, S. S., Guruvayoorappan, C., Sakthivel, K. M. & Rasmi, R. R. Ki-67 protein as a tumour proliferation marker. *Clin. Chim. Acta* **491**, 39–45 (2019).

Acknowledgements

The authors thank Dr. Mark Minden and Ruijuan He (Princess Margaret Cancer Center, University Health Network, Toronto, Canada) for their help in transfecting the BxPC3-DsRed cell line with the 5xHRE/GFP reporter. Napoleon Law and Feryal Sarraf (STTARR Pathology, University Health Network, Toronto, Canada) processed and stained all tumor tissue sections. James Jonkman (Advanced Optical Microscopy Facility, University Health Network, Toronto, Canada) provided valuable guidance and discussion for all microscopy experiments.

Author contributions

T.S., S.R. and R.S.D. developed the concept for this study. T.S. performed all animal surgeries, image processing and data analysis. P.L. performed radiation treatment planning and dosimetry. T.S. and S.R. performed in vivo irradiation and imaging experiments. T.S. wrote the manuscript. All authors edited the manuscript and approved the final version.

Declarations

Competing interests

The authors declare no competing interests.

Data availability

The data generated in this study are available from the corresponding author upon reasonable request.

Additional information

Correspondence and requests for materials should be addressed to R.S.D.

Reprints and permissions information is available at www.nature.com/reprints.

Publisher's note Springer Nature remains neutral with regard to jurisdictional claims in published maps and institutional affiliations.

Open Access This article is licensed under a Creative Commons Attribution-NonCommercial-NoDerivatives 4.0 International License, which permits any non-commercial use, sharing, distribution and reproduction in any medium or format, as long as you give appropriate credit to the original author(s) and the source, provide a link to the Creative Commons licence, and indicate if you modified the licensed material. You do not have permission under this licence to share adapted material derived from this article or parts of it. The images or other third party material in this article are included in the article's Creative Commons licence, unless indicated otherwise in a credit line to the material. If material is not included in the article's Creative Commons licence and your intended use is not permitted by statutory regulation or exceeds the permitted use, you will need to obtain permission directly from the copyright holder. To view a copy of this licence, visit http://creativecommons.org/licenses/by-nc-nd/4.0/.

© The Author(s) 2024